

# Free Energy Profile and Kinetics Studies of Paclitaxel Internalization from the Outer to the Inner Wall of Microtubules

Giorgio Maccari,<sup>†</sup> Mattia Mori,<sup>‡,†</sup> Javier Rodríguez-Salarichs,<sup>§,||</sup> Weishuo Fang,<sup>⊥</sup> José Fernando Díaz,<sup>§</sup> and Maurizio Botta\*,<sup>†</sup>

<sup>†</sup>Dipartimento Farmaco-Chimico Tecnologico, Facoltà di Farmacia, Università degli Studi di Siena, I-53100 Siena, Italy

<sup>‡</sup>Dipartimento di Chimica e Tecnologia del Farmaco, Università di Roma “La Sapienza”, I-00185 Roma, Italy

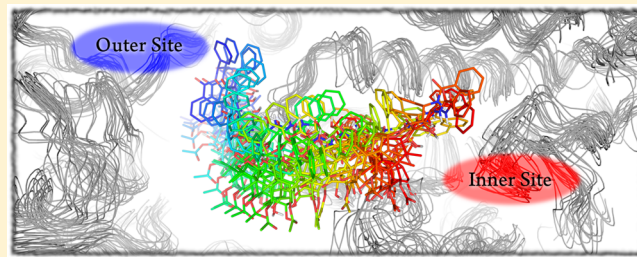
<sup>§</sup>Centro de Investigaciones Biológicas, CSIC, 28040 Madrid, Spain

<sup>||</sup>Centro de Estudios Avanzados de Cuba, La Lisa, Ciudad Habana 17100, Cuba

<sup>⊥</sup>Institute of Materia Medica, Chinese Academy of Medical Sciences, Beijing 100050, China

## Supporting Information

**ABSTRACT:** Several pieces of experimental evidence led us to hypothesize that the mechanism of action of paclitaxel (Taxol) could involve a two-steps binding process, with paclitaxel first binding within the outer wall of microtubules and then moving into the inner binding site. In this work, we first used multiply targeted molecular dynamics (MTMD) for steering paclitaxel from the outer toward the inner binding site. This rough trajectory was then submitted to a refinement procedure in the path collective variables space. Paclitaxel binding energy was monitored along the refined pathway, highlighting the relevance of residues belonging to the H6–H7 and the M-loops. Computational results were supported by kinetics studies performed on fluorescent paclitaxel derivatives.



## INTRODUCTION

Paclitaxel is an anticancer natural substance isolated and characterized in 1960s from the bark extract of *Taxus brevifolia* (Figure 1).<sup>1</sup> In 1992, paclitaxel was approved by the U.S. Food and Drug Administration for the treatment of ovarian cancer,<sup>2</sup> and in 1994 for the treatment of metastatic breast carcinoma.<sup>3</sup> Since then, paclitaxel has been used for the clinical treatment of several different cancers, among which are the HIV-associated Kaposi's sarcoma, small-cell lung cancer, and squamous cell cancers of the head and neck.<sup>4–6</sup> From structural and functional

standpoints, paclitaxel binds on  $\alpha/\beta$ -tubulin heterodimers and acts as a microtubule stabilizing agent (MSA) by inhibiting microtubules dynamic instability and enhancing tubulin polymerization, which, in turn, promotes mitotic arrest and apoptosis.<sup>7</sup> This novel mechanism of action was first described for paclitaxel<sup>8</sup> and is currently shared by chemically diverse MSAs that target at least two different binding sites.<sup>9–11</sup> The paclitaxel binding mode toward assembled tubulin heterodimers was characterized in 1998 by means of electron crystallography,<sup>12,13</sup> showing the binding site located on the luminal wall of the  $\beta$  subunit. Although this binding site agreed with most of the results previously obtained with photolabeling taxanes,<sup>14–18</sup> it did not correlate with the higher affinity observed for paclitaxel toward microtubules than to isolated heterodimers, as well as with the evidence that some azido derivatives of paclitaxel interact with the  $\alpha$ -subunit.<sup>15,19</sup>

In 2000, Diaz and co-workers supposed that the paclitaxel binding on microtubules was kinetically too fast for compatibility with a direct interaction within the inner binding site,<sup>20</sup> and they performed kinetic studies that revealed a two-steps binding mechanism, which led to the hypothesis of the existence of an easily accessible binding site, located on the outer wall of microtubules.<sup>21–23</sup> In previous works, we modeled the outer binding site in complex with paclitaxel,<sup>24,25</sup> suggesting

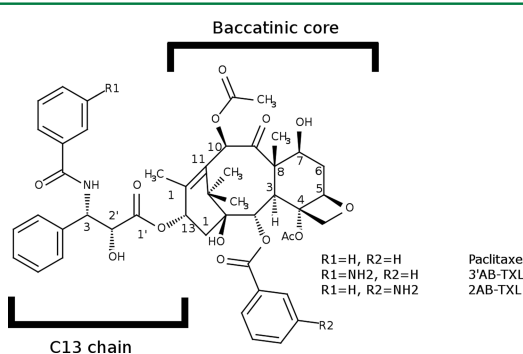


**Figure 1.** Chemical structure of paclitaxel and its fluorescent derivatives. The canonical numbering of the baccatinic core and the C13 chain position is reported.

Received: July 30, 2012

Published: November 6, 2012

a possible binding mode of paclitaxel that was in agreement with the residual binding of taxanes to the  $\alpha$ -subunit, as observed by photolabeling studies.<sup>15,19</sup> Notably, tubulin residues contacted by paclitaxel in our model were also recently highlighted by NMR studies.<sup>26</sup> See Figure 2 for a representation of the system studied in this work.

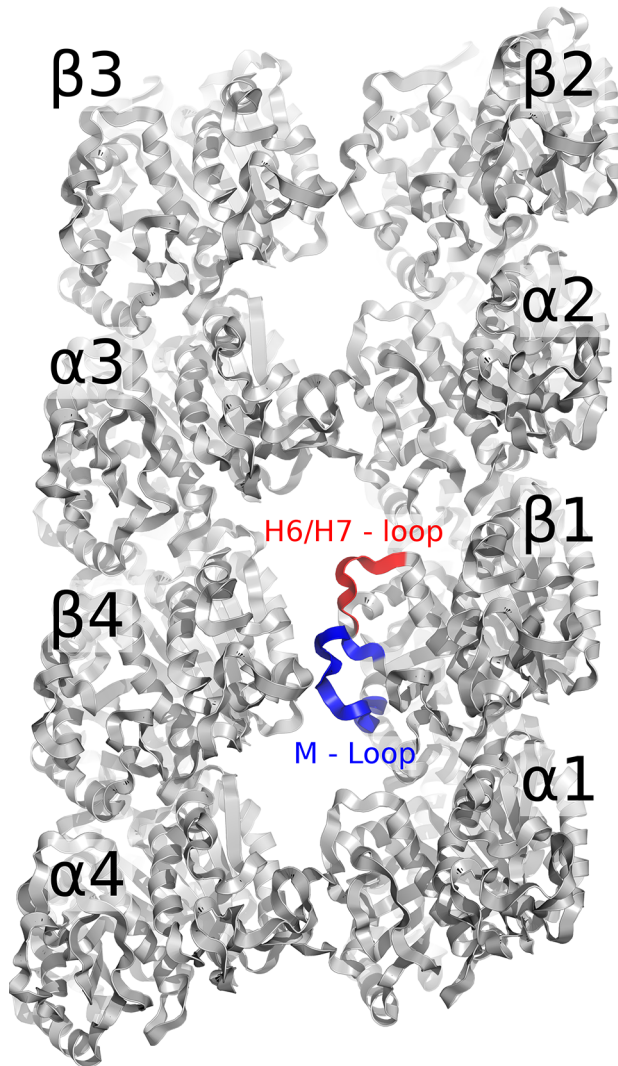


**Figure 2.** Cartoon representation of a microtubule slice. The system studied in this work is composed of  $\alpha_2$ ,  $\alpha_3$ ,  $\beta_1$ , and  $\beta_4$  subunits. The view is taken from the microtubule lumen; H6/H7 and M-loops are highlighted as red and blue cartoons, respectively.

The hypothesis we recall in this work is that paclitaxel first binds to the outer site and then is internalized. We used multiply targeted molecular dynamics (MTMD) to generate a rough pathway for the internalization of paclitaxel from the outer to the inner site, which was further refined in the path collective variables space. The energetic profile of the internalization process and the refined paclitaxel binding conformations provided insights into the paclitaxel mechanism of action, which could be exploited to design derivatives endowed with improved efficacy. Finally, the reliability of the model was supported by experimental data on the kinetics of internalization measured for two sample fluorescent paclitaxel derivatives.

## RESULTS AND DISCUSSION

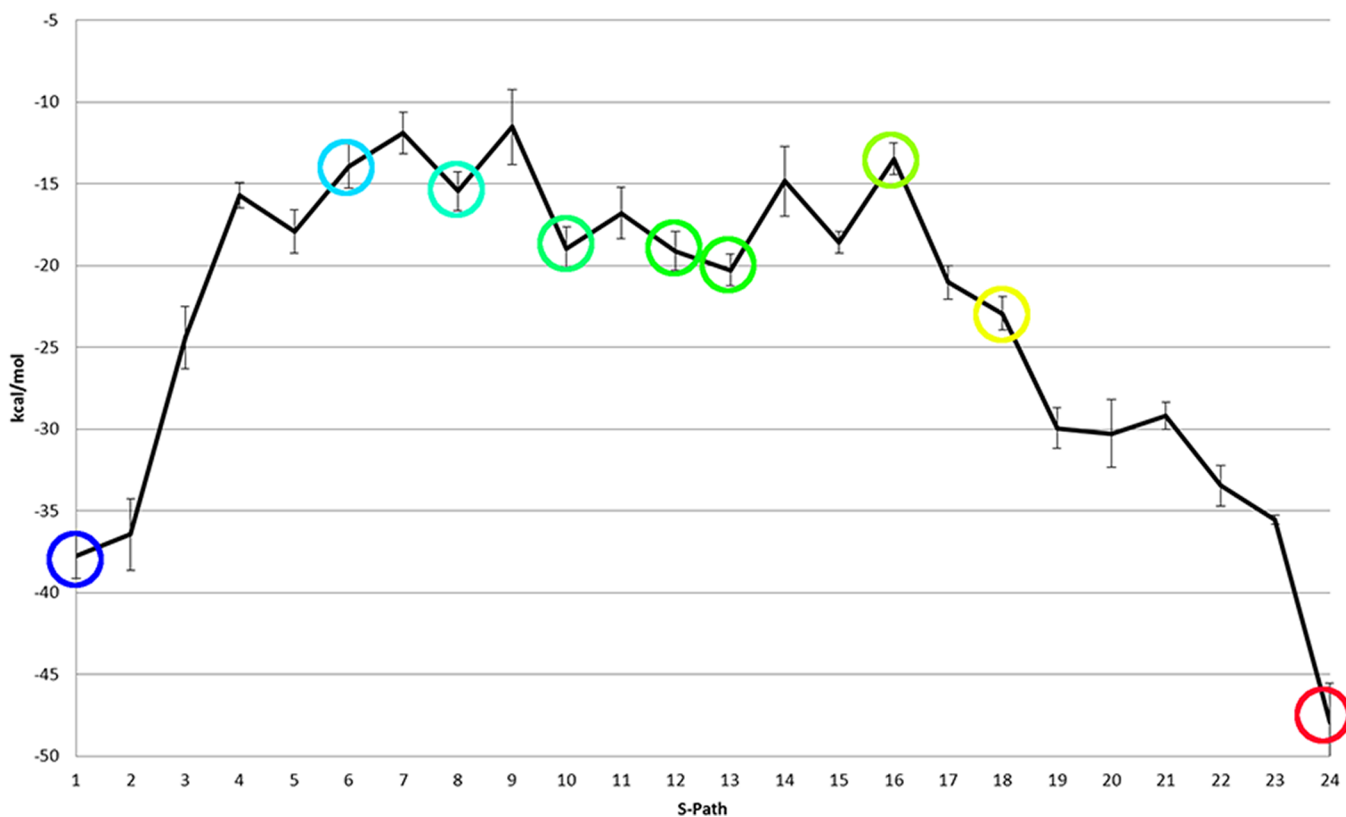
### Generation of Reference Structures for MTMD.

Coordinates of the tubulin tetramer in complex with paclitaxel bound to the inner site were kindly provided by Professor Pablo Chacón from The Scripps Research Institute,<sup>27</sup> whereas coordinates of the tubulin tetramer with paclitaxel bound to the outer site were retrieved from the previous computational study.<sup>24</sup> These two structures were relaxed by means of classic molecular dynamics (MD) simulations with the program AMBER11.<sup>28–30</sup> Both complexes were stable during MD simulations (see the Supporting Information). The paclitaxel delta energy of binding was calculated with the MM/GBSA method<sup>31–33</sup> and was sizably lower within the inner site ( $-47.94 \pm 2.40$  kcal/mol) than within the outer site ( $-37.77 \pm 1.33$  kcal/mol), suggesting a possible enthalpic gain from paclitaxel internalization. The frame with the lowest root mean squared deviation (RMSD) from the average MD structure was considered as representative of each MD trajectory and was selected for the further analysis. Centroids of paclitaxel in the two binding sites were separated by 26.8 Å, and these two structures were differing mainly in the conformation and relative orientation of the H6/H7- and the M-loops. When paclitaxel was on the outer site, a salt bridge between R278 $\beta$  of the M-loop and D226 $\beta$  of helix H7 partially hindered the accessibility toward the inner site. Conversely, when paclitaxel was on the inner site, the H6/H7-loop was turned toward the microtubule lumen in contact with the ligand, as observed either by MD simulations and electron crystallography.

### Multiply Targeted Molecular Dynamics.

To investigate the internalization process of paclitaxel, we first generated a rough pathway by means of multiply targeted molecular dynamics (MTMD), a computational method that adds additional energy terms to the potential function based on the RMSD between the actual structure and a reference one.<sup>34–36</sup> Since MTMD permits the application of different steering forces to different groups of residues, it was selected to simulate the conformational changes oriented at promoting the internalization of paclitaxel, namely, the opening of the M-loop and the crossing of the gatekeeper H6/H7-loop.<sup>23,37</sup> In fact, in a preliminary analysis, the application of a single steering force was not capable of simulating the whole internalization process. The weakest steering forces were chosen to avoid the generation of possible artifacts and were applied to two different groups of residues of the system. The first group was composed of paclitaxel and residues of the inner site and was subjected to a constant force of  $0.5 \text{ kcal}\cdot\text{mol}^{-1}\cdot\text{\AA}^{-2}$  during the whole simulation time. Conversely, the second group was composed by the M-loop, which was steered by a force of  $0.5 \text{ kcal}\cdot\text{mol}^{-1}\cdot\text{\AA}^{-2}$  only during the central part of the simulation.

It is to be noted that a similar work has been previously reported by Tuszyński and co-workers,<sup>38</sup> who generated a possible pathway for paclitaxel internalization by using 1 ns of targeted molecular dynamics (TMD) simulations, starting from a paclitaxel conformation that is significantly different from that described here. Despite the pioneering role of that work, we feel that a longer simulation time could provide a more accurate description of the trajectory. For this reason, we simulated six different independent replicas of the internalization process lasting 10 ns each one. Moreover, the paclitaxel binding conformation, which corresponds to the starting point of our MTMD simulation, has been supported by experimental studies<sup>25</sup> and is in agreement with structural data discussed.

MM/GBSA  $\Delta\Delta G$  as function of S-Path

**Figure 3.** Profile of the paclitaxel delta energy of binding along the internalization pathway. X-axis: checkpoints number. Y-axis: the delta energy of binding expressed in kcal/mol. The binding conformation of paclitaxel at checkpoints highlighted with colored circles is reported in Figure 4 (the same color code is applied).

Visual analysis of MTMD trajectories revealed that the C13 chain (Figure 1) promotes the paclitaxel internalization by performing hydrophobic and polar interactions with residues of the H6/H7- and M-loops, whereas the baccatinic moiety was hampered by steric hindrance. The benzoyl group at C2 remained anchored to the outer site for 2.5 ns then, by interacting with H6/H7-loop, it promoted the rotation of the paclitaxel molecule to adopt an orientation suitable for binding to the inner site.

**Refinement Procedure.** The rough paclitaxel internalization pathway was first generated by means of MTMD, by applying steering forces that moved paclitaxel from the outer to the inner site. One may note that the application of steering forces could produce artifactual trajectories, even though the weakest forces as possible were applied to prevent large conformational distortions. Hence, with the aim of providing a refined energetic and conformational profile for the paclitaxel internalization pathway, MTMD trajectories were further submitted to a refinement procedure within the S- and Z-path collective variables space.<sup>39–43</sup> The refinement procedure was performed by using the PLUMED plug-in for AMBER11,<sup>44</sup> which requires a set of checkpoint structures, equally spaced in term of RMSD, connecting the starting and the ending conformations of the pathway. To extract this set of equidistant checkpoints from trajectories, we have iteratively alternated a refinement procedure in the path collective variables space to frame selection, performed with a genetic algorithm that has been implemented into an in-house Python script. The algorithm optimizes the string tension applied to the set of

checkpoints. At every refinement cycle, an umbrella-like potential was applied at the integer values of the S-path, whereas paclitaxel was kept within its trajectory by a wall potential applied on the Z-path. Each refinement cycle was performed on the set of 24 checkpoints selected from the previous run. This refinement procedure was iterated 7 times, until geometry convergence was reached ( $\text{RMSD} < 0.5 \text{ \AA}$ ).

To outline the energetic profile of paclitaxel along the pathway, the paclitaxel delta energy of binding was calculated on the final set of refined checkpoints by means of the MM/GBSA method. A significant energetic barrier was observed from checkpoint 4 to 9 (see Figure 3). Checkpoints with the highest paclitaxel delta energy of binding correspond to the crossing of the H6/H7-loop.

The paclitaxel binding mode at every checkpoint was visually inspected (Figure 4). At checkpoints 1 and 2, paclitaxel was stabilized within the outer binding site by the same set of interactions already observed during preliminary MD simulations (Figure 4 checkpoint 1), to reinforcing the robustness of the initial model. From checkpoint 3 to 6, the C13 chain start moving toward the microtubule lumen, a process that was associated with a significant increase in the delta energy of binding. On the contrary, the benzoyl group at C2 performed usual hydrophobic interaction with residues of the outer site belonging to the  $\beta$  subunit, while the oxetane ring was in H-bond distance (2.7 Å) with the hydroxyl group of T220 $\beta$  (Figure 4 checkpoint 6). Checkpoints with the highest paclitaxel delta energy of binding energy can be considered the critical step of the internalization process. The formation of

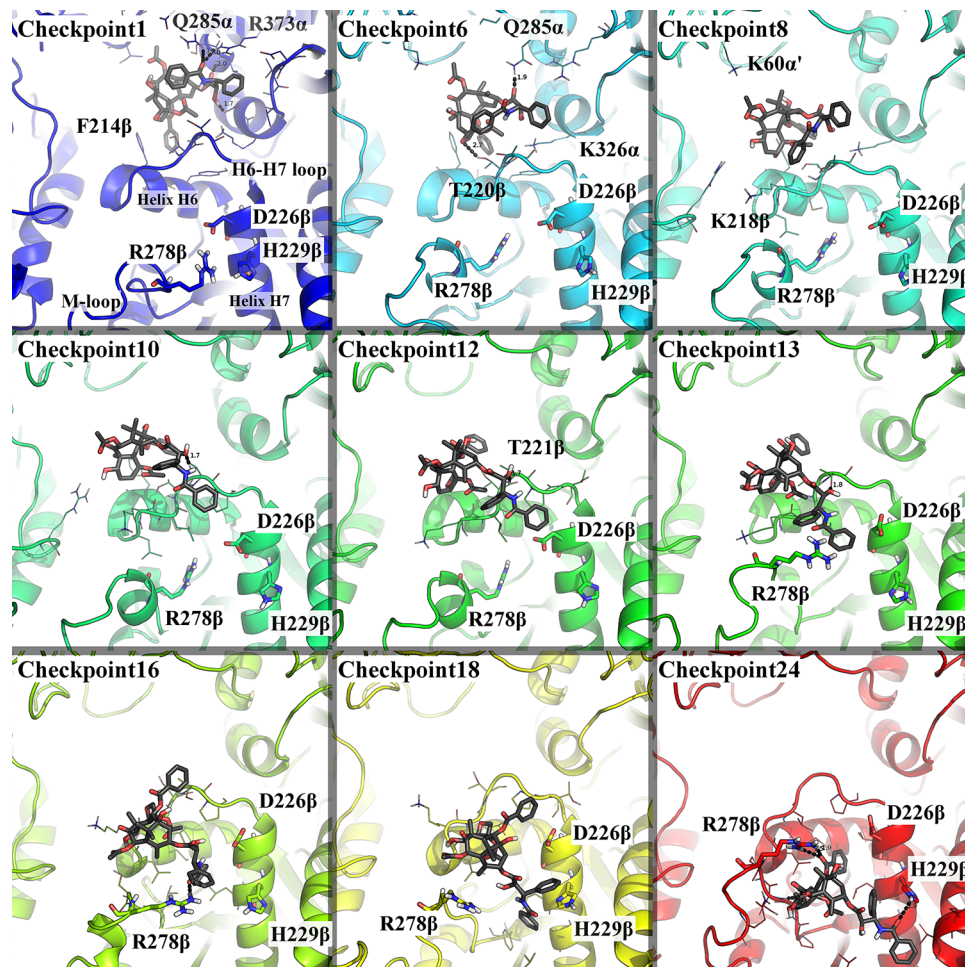


**Figure 4.** Binding conformation of paclitaxel in representative checkpoints. Tubulin is showed as cartoons, paclitaxel as gray sticks. Residues, which are located in a range of 5 Å from paclitaxel, are showed as lines. H-bond interactions are shown as black dashes (an enlarged version of each panel is available in the Supporting Information). The checkpoint number is reported at the upper-left corner of each panel, where selected checkpoints correspond to those highlighted with colored circles in Figure 3. For the sake of clarity, the H6/H7-loop and helices H6 and H7 are labeled only in the first panel. The orientation of the tubulin system is constant in all panels.

H-bond interactions between paclitaxel oxetane ring and T220 $\beta$  hydroxyl group (2.7 Å) and between the hydroxyl group at position 2' and the side chain of T221 $\beta$  (about 1.8 Å) allowed paclitaxel to cross the H6/H7-loop and to approach the inner binding site. Starting from checkpoint 10, paclitaxel was in contact with the inner wall of microtubule, although the acetyl group at C10 was still in contact with the H6/H7 loop, which adopted its final conformation (Figure 4 checkpoints 10, 12, and 13). The stability of the complex increased progressively after checkpoint 13, when the C13 chain approached toward the inner site by interfering with a salt bridge between R278 $\beta$  and D226 $\beta$  thus opening the M-loop. The formation of an H-bond interaction (2.9 Å) between H229 $\beta$  and the amide moiety at 3' position of paclitaxel completed paclitaxel internalization (Figure 4 checkpoint 24). An enlarged version of each checkpoint conformation shown in Figure 4 is available in the Supporting Information.

**Kinetic Studies.** To further support the reliability of the computational model, the kinetics of internalization of two fluorescent taxane derivatives was studied using stopped flow techniques.<sup>45,46</sup> The 2-debenzoyl-2-(*m*-aminobenzoyl) paclitaxel (2AB-TXL) and 3'-N-*m*-aminobenzamido-3'-N-debenzamido paclitaxel (3'AB-TXL) were selected for this study. These molecules are featured by a small modification of the paclitaxel

structure, namely, an amino group at position meta of the 2 and 3' benzoyl moieties (Figure 1).

The kinetics of binding of these compounds to the microtubules was analyzed using a two steps mechanism of internalization, taking into account binding of the fluorescent compounds to the unassembled dimers, which are present in solution. Three equilibrium states were concurrently considered:



where LIG is the free ligand, MTBX are microtubules, DIM free heterodimers, LIG-MTBX-EXT is the ligand bound to the outer site, LIG-MTBX-INT is the ligand bound to the inner site, and LIG-DIM is the ligand bound to the dimer.

This kinetics model fits the experimental data, allowing for the calculation of the concentrations for the compound bound to the inner and the outer site (See Figure 12S in the Supporting Information) and indicates that the compound 3'AB-TXL internalizes faster (the forward rate constant of reaction II  $k_+$  is considered to be the rate constant of internalization)  $k_{\text{int}}(2\text{AB-TXL}) = 4 \pm 2 \text{ s}^{-1}$  versus  $k_{\text{int}}(3'\text{AB-TXL}) = 1.5 \pm 0.5 \text{ s}^{-1}$ .

$\text{TXL}) = 7 \pm 1 \text{ s}^{-1}$ . Note that although the total time needed for the compound 2AB-TXL to reach the inner site is shorter, this is due to its higher binding rate constant to the outer binding site (Figure 5).

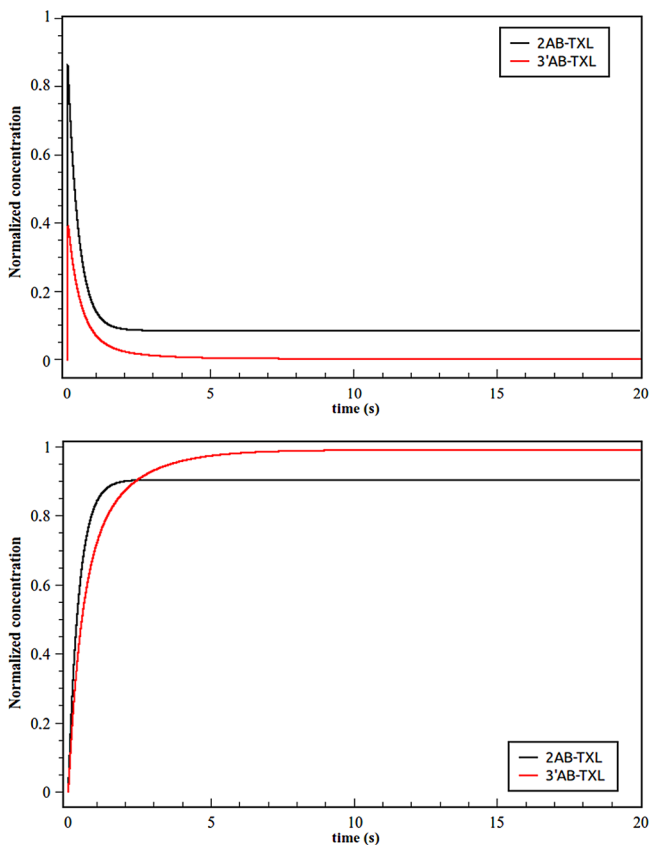


**Figure 5.** Evolution of the concentrations of 2AB-TXL and 3'AB-TXL bound to the external (top graph) or the internal (bottom graph) binding site during the course of the experiment.

### Comparison between Kinetic and Computational Data.

The binding conformations of 2AB-TXL and 3'AB-TXL along the internalization pathway were generated by substituting the aromatic hydrogen atom of paclitaxel in all checkpoints of the refined set with the amino group (the chemical structures of 2AB-TXL and 3'AB-TXL are reported in Figure 1). Resulting complexes were then energy minimized, and the ligand delta energy of binding was calculated by means of the MM/GBSA method. We generated two sets of binding modes for each derivative, accounting for the different orientations of the amino group substituted in the two possible meta positions of the phenyl ring, albeit the set showing the lowest delta energy of binding was considered for further speculations and reported in the graph of Figure 6.

The delta energy of binding within the inner site was similar for both compounds. However, the 3'AB-TXL seems to perform more profitable interactions with tubulin during the internalization pathway than the 2AB-TXL. The experimentally derived kinetic profiles reported in Figure 5 were then compared with computational data obtained for 2AB-TXL and 3'AB-TXL. The lower interaction energy calculated for 3'AB-TXL by means of this computational protocol is in agreement with its higher kinetic constant experimentally observed, since 3'AB-TXL is internalized faster than 2AB-TXL.

The ability of our model to explain biochemical data, especially for slightly different paclitaxel derivatives, strongly support the internalization mechanism herein proposed and studied by MTMD simulation and umbrella-like refinement.

Finally, our computational model is also in agreement with the structure–activity relationship (SAR) of paclitaxel derivatives modified at positions 2 and 3', highlighting the importance of these groups for the affinity of taxanes to tubulin. In fact, the removal or the dearomatization of the benzoyl group at position 2 led to the loss of activity, while modification of the amide at position 3' could lead to more active taxanes, such as docetaxel.<sup>47–49</sup>

### CONCLUDING REMARKS

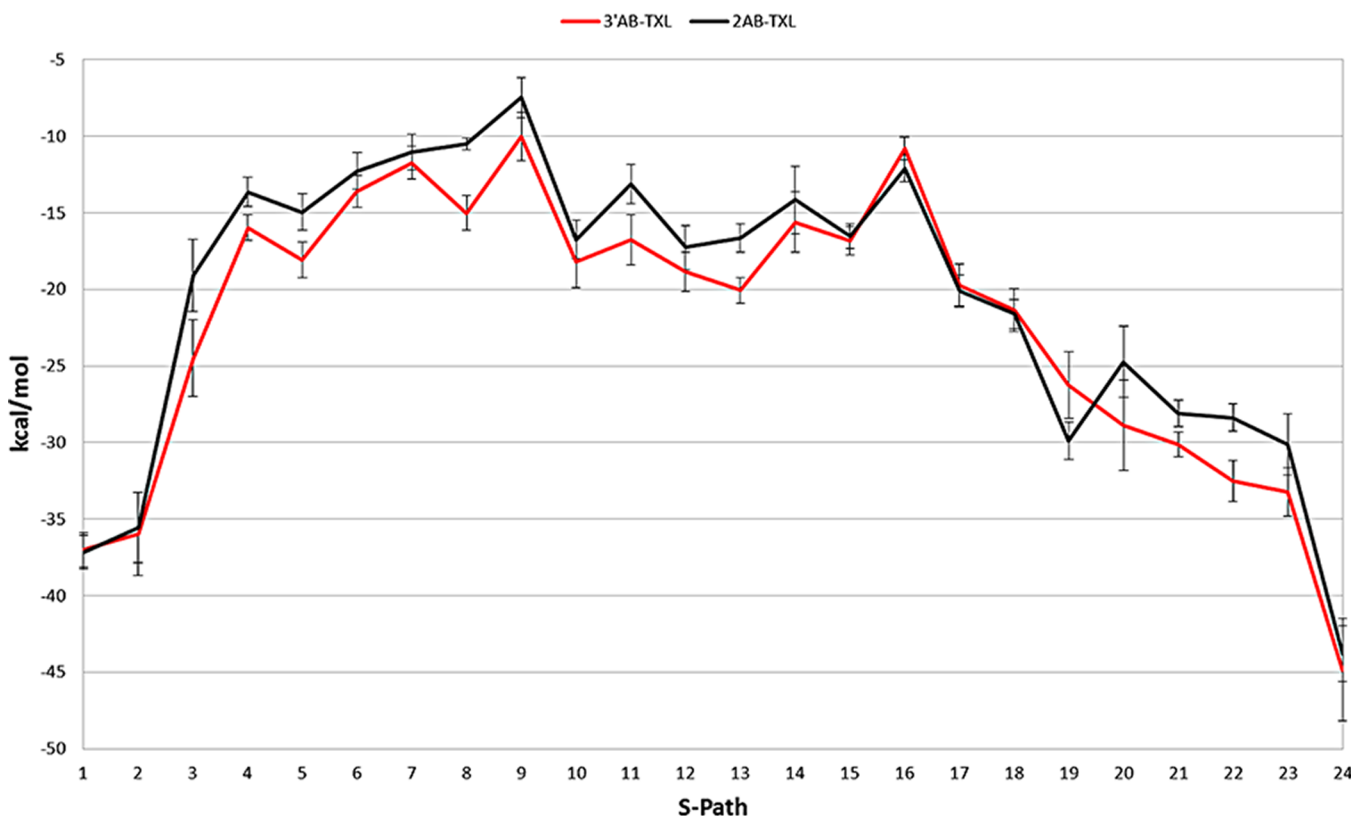
Enhanced sampling methods have been used to model the internalization of paclitaxel from the outer and easily accessible binding site to the inner one, which is known from electron crystallography. The rough trajectory was obtained by means of MTMD and was further refined in the path collective variables. The energetic profile of paclitaxel was investigated by means of the MM/GBSA method. Our results are able to explain the different kinetics of internalization observed for two samples paclitaxel derivatives. The agreement between experimentally determined kinetic data and the predicted energetic profile support that the internalization process could be enthalpy-driven.

This refined computational protocol could be used to rationally design novel paclitaxel derivatives endowed with a faster kinetic of internalization, as well as with a higher potency as anticancer leads. Moreover, the protocol here discussed could be used to study different microtubule stabilizing agents such as epothilones, providing more insight on their mechanism of action.

### EXPERIMENTAL SECTION

**Molecular Dynamics Protocol.** The same MD protocol was used to relax the tubulin in complex with paclitaxel within the outer and the inner site. Paclitaxel and cofactors were parametrized as reported elsewhere.<sup>25</sup> Topology files were prepared with Leap<sup>50</sup> using the ff03 forcefield.<sup>50</sup> A total of 48 Na<sup>+</sup> counterions were added to balance the total charge of the system. A box of TIP3P water molecules was added with a buffer of 8.0 Å.<sup>51</sup> MD simulations were performed with AMBER11,<sup>30</sup> using a cutoff of 15 Å, time step 1 fs, and the SHAKE algorithm to constraint bonds involving hydrogen atoms.<sup>52,53</sup> The energy minimization was initially performed for the solvent, keeping the solute frozen, for 1000 steps using the steepest descent algorithm (SD) followed by 3000 steps with the conjugate gradient algorithm (CG). Then, the solute was minimized for 3000 steps SD and 3000 steps CG, keeping the solvent frozen. Finally, the solvated system was relaxed for 3000 steps SD and 7000 steps CG. The system was heated from 0 to 300 K for 0.25 ns using the Langevin thermostat; then, the other 0.25 ns at constant pressure were used to equilibrate the density before to equilibrate the system for 0.5 ns. The final production phase of MD lasted 1 ns without any restraint.

The delta energy of binding of paclitaxel within the inner and outer binding sites was estimated by means of the MM/GBSA method, by using 500 frames of the unrestrained MD, with a salt concentration of 0.1 M and using the generalized Born model modification developed by Onufriev et al.<sup>54,55</sup>

MM/GBSA  $\Delta\Delta G$  as function of S-Path

**Figure 6.** MM/GBSA delta energy of binding of 2AB-TXL (black line) 3'AB-TXL (red line) and along the S-Path.

**Multiply Targeted Molecular Dynamics.** Multiply targeted molecular dynamics (MTMD) simulations were performed by using the representative frames of the two MD of the outer and the inner binding site as starting and end point, respectively. The run time was 10 ns with time step of 1 fs. The SHAKE algorithm was applied to constraint bonds involving hydrogen atoms.<sup>52,53</sup> Two restraint masks were applied: the first including paclitaxel and residues of the inner binding site; the second including the M-loop.

On the first mask a constant force of 0.5 kcal·mol<sup>-1</sup>·Å<sup>-2</sup> was applied, with a target RMSD that decreases linearly to 0.5 Å during the simulation. Residues of the second mask were steered with a restraint force that increased linearly from 0 to 0.5 kcal·mol<sup>-1</sup>·Å<sup>-2</sup> from nanoseconds 3.5 to 4.0, was stable for 3.0 ns and progressively decreased to 0 kcal·mol<sup>-1</sup>·Å<sup>-2</sup> from nanoseconds 7.0 to 7.5.

Six independent MTMD replicas were performed. Four out of the six replicas showed a paclitaxel binding conformation within the inner site comparable with that described by MD (RMSD < 2.5 Å), one of these has a paclitaxel RMSD lower than 1.5 Å and was selected for next steps.

**Refinement Procedure.** The MTMD trajectory showing the lowest RMSD for paclitaxel binding within the inner site with respect to the binding conformation described by MD was selected for the refinement procedure. The optimization of the 24 frames describing the pathway was performed by alternating exhaustive conformational sampling runs and frame selection. Each conformational sampling run was conducted over the frame selected for the previous run, by applying an umbrella-like potential of 5.0 kcal/mol on the S-path and a wall constraint of 25.0 kcal/mol on the Z-path at the value of 1.0

(units of Z-path). For each frame, the simulation time was 1 ns with a time step of 1 fs. Calculations were done using the PLUMED (v 1.3) plugin for AMBER11.<sup>44</sup>

To select equidistant frames at the end of each run, an in-house Python script was used. The script implements a genetic algorithm that evaluates multiple sets of frames while minimizing the  $E_{NET}$  term described in Branduardi et al. 2007.<sup>42</sup>

**Kinetic Studies.** The kinetics of internalization of 2AB-TXL<sup>45</sup> and 3'AB-TXL<sup>46</sup> in preassembled stabilized microtubules<sup>21,56</sup> have been determined by mixing 5 μM paclitaxel binding sites with 1 μM of the desired ligand at 25 °C using a Bio-Logic SF300S stopped flow device equipped with a fluorescence detection system with an excitation wavelength of 313 nm and a filter with a cutoff of 380 nm in the emission pathway. Appropriate photobleaching controls were done.

The experimental kinetic curves were fitted to a two steps mechanism of binding (taking into account the binding of the ligands to the 12% percentage of unassembled tubulin) using COPASI 4.8.<sup>57</sup> All binding constants, on/off rate of binding to the external site in microtubules and on/off rate of binding to the free dimers, and the internalization and externalization rates were optimized by minimizing (employing evolutionary programming method implemented in the software) the root-mean-square deviation between the experimental and the calculated fluorescence curves. Then, the concentration of each species during the internalization process can be calculated considering the optimized on/off rates over a given time interval (in our case 25 min, timeout to reach the chemical equilibrium). A deterministic time course simulation was performed using a numerical integration of ordinary differential

equations (eqs 1–5) with a fourth order Runge–Kutta, LSODA algorithm.<sup>58,59</sup> The default parameters set was used.

$$\begin{aligned} \frac{d([LIG\text{-}MTBX\text{-}EXT])}{dt} &= (k_{1(\text{step1})}[LIG][MTBX] - k_{2(\text{step1})}[LIG\text{-}MTBX\text{-}EXT]) \\ &\quad - (k_{1(\text{step2})}[LIG\text{-}MTBX\text{-}EXT] \\ &\quad - k_{2(\text{step1})}[2AB\text{-}MTBX\text{-}INT]) \end{aligned} \quad (1)$$

$$\begin{aligned} \frac{d([LIG])}{dt} &= -(k_{1(\text{step1})}[LIG][MTBX] \\ &\quad - k_{2(\text{step1})}[LIG\text{-}MTBX\text{-}EXT]) \\ &\quad - (k_{1(\text{step3})}[LIG][DIM] \\ &\quad - k_{2(\text{step3})}[LIG\text{-}DIM]) \end{aligned} \quad (2)$$

$$\begin{aligned} \frac{d([MTBX])}{dt} &= -(k_{1(\text{step1})}[LIG][MTBX] \\ &\quad - k_{2(\text{step1})}[LIG\text{-}MTBX\text{-}EXT]) \end{aligned} \quad (3)$$

$$\begin{aligned} \frac{d([LIG\text{-}MTBX\text{-}INT])}{dt} &= (k_{1(\text{step2})}[LIG\text{-}MTBX\text{-}EXT] \\ &\quad - k_{2(\text{step1})}[LIG\text{-}MTBX\text{-}INT]) \end{aligned} \quad (4)$$

$$\begin{aligned} \frac{d([LIG\text{-}DIM])}{dt} &= (k_{1(\text{step3})}[LIG][dim] \\ &\quad - k_{2(\text{step3})}[LIG\text{-}DIM]) \end{aligned} \quad (5)$$

## ASSOCIATED CONTENT

### Supporting Information

RMSD analysis of MD simulations; enlarged versions of panels presented in Figure 4; Figure showing experimental data for the kinetics of binding of 2AB-TXL and 3'AB-TXL to 5 μM paclitaxel binding sites in stabilized microtubules. This material is available free of charge via the Internet at <http://pubs.acs.org>.

## AUTHOR INFORMATION

### Corresponding Author

\*E-mail: botta.maurizio@gmail.com.

### Notes

The authors declare no competing financial interest.

## ACKNOWLEDGMENTS

Profitable discussions with Andrea Cavalli are acknowledged with gratitude. We thank Matadero Municipal Vicente de Lucas de Segovia for the calf brains for tubulin purification. J.R.S. was supported by a fellowship from Programa de Cooperación Científica entre el Ministerio de Ciencia, Tecnologías y Medio Ambiente de la República de Cuba (CITMA) y el CSIC. This work was supported in part by Grant Nos. BIO2010-16351 and CTQ2009-08536 from Ministerio de Economía y Competitividad (to J.F.D. and J.J.B., respectively) and Grant No. S2010/BMD-2457 BIPEDD2 from Comunidad Autónoma de Madrid to JFD. We also thank the Natural Science Foundation of China (NSFC), Grant No. 30930108.

## ABBREVIATIONS

MD, molecular dynamics; TMD, targeted molecular dynamics; MTMD, multiply targeted molecular dynamics; MM/GBSA, molecular mechanics/generalized born surface area; RMSD, root mean squared deviation; FES, free energy surface; 2AB-TXL, 2-debenzoyl-2-(m-aminobenzoyl) paclitaxel; 3'AB-TXL, 3'-N-m-aminobenzamido-3'-N-debenzamido paclitaxel; MTBX, stabilized microtubules; DIM, tubulin heterodimer; SAR, structure–activity relationship; SD, steepest decent; CG, conjugate gradient

## REFERENCES

- (1) Wani, M. C.; Taylor, H. L.; Wall, M. E.; Coggon, P.; McPhail, A. T. Plant Antitumor Agents. VI. The Isolation and Structure of Taxol, a Novel Antileukemic and Antitumor Agent from *Taxus Brevifolia*. *J. Am. Chem. Soc.* **1971**, *93*, 2325–2327.
- (2) Eisenhauer, E. A.; Vermorken, J. B. The Taxoids. Comparative Clinical Pharmacology and Therapeutic Potential. *Drugs* **1998**, *55*, 5–30.
- (3) Crown, J.; O’Leary, M. The Taxanes: An Update. *Lancet* **2000**, *355*, 1176–1178.
- (4) Saville, M. W.; Lietzau, J.; Pluda, J. M.; Feuerstein, I.; Odom, J.; Wilson, W. H.; Humphrey, R. W.; Feigal, E.; Steinberg, S. M.; Broder, S. Treatment of HIV-Associated Kaposi’s Sarcoma with Paclitaxel. *Lancet* **1995**, *346*, 26–28.
- (5) Welles, L.; Saville, M. W.; Lietzau, J.; Pluda, J. M.; Wyvill, K. M.; Feuerstein, I.; Figg, W. D.; Lush, R.; Odom, J.; Wilson, W. H.; Fajardo, M. T.; Humphrey, R. W.; Feigal, E.; Tuck, D.; Steinberg, S. M.; Broder, S.; Yarchoan, R. Phase II Trial with Dose Titration of Paclitaxel for the Therapy of Human Immunodeficiency Virus-Associated Kaposi’s Sarcoma. *J. Clin. Oncol.* **1998**, *16*, 1112–1121.
- (6) Kim, S. Y.; Kim, D. H.; Lee, H. J.; Seo, Y. J.; Lee, J. H.; Lee, Y. Treatment of Disseminated Classic Type of Kaposi’s Sarcoma with Paclitaxel. *Ann Dermatol* **2011**, *23*, 504–507.
- (7) Schiff, P. B.; Fant, J.; Horwitz, S. B. Promotion of Microtubule Assembly in Vitro by Taxol. *Nature* **1979**, *277*, 665–667.
- (8) Jordan, M. A.; Toso, R. J.; Thrower, D.; Wilson, L. Mechanism of Mitotic Block and Inhibition of Cell Proliferation by Taxol at Low Concentrations. *Proc. Natl. Acad. Sci. U.S.A.* **1993**, *90*, 9552–9556.
- (9) Pryor, D. E.; O’Brate, A.; Bilcer, G.; Díaz, J. F.; Wang, Y.; Wang, Y.; Kabaki, M.; Jung, M. K.; Andreu, J. M.; Ghosh, A. K.; Giannakakou, P.; Hamel, E. The Microtubule Stabilizing Agent Laulimalide Does Not Bind in the Taxoid Site, Kills Cells Resistant to Paclitaxel and Epothilones, and May Not Require Its Epoxide Moiety for Activity. *Biochemistry* **2002**, *41*, 9109–9115.
- (10) Buey, R. M.; Barasoain, I.; Jackson, E.; Meyer, A.; Giannakakou, P.; Paterson, I.; Mooberry, S.; Andreu, J. M.; Diaz, J. F. Microtubule Interactions with Chemically Diverse Stabilizing Agents: Thermodynamics of Binding to the Paclitaxel Site Predicts Cytotoxicity. *Chem. Biol.* **2005**, *12*, 1269–1279.
- (11) Gaitanos, T. N.; Buey, R. M.; Díaz, J. F.; Northcote, P. T.; Teesdale-Spittele, P.; Andreu, J. M.; Miller, J. H. Peloruside A Does Not Bind to the Taxoid Site on β-Tubulin and Retains Its Activity in Multidrug-Resistant Cell Lines. *Cancer Res.* **2004**, *64*, 5063–5067.
- (12) Nogales, E.; Wolf, S. G.; Downing, K. H. Structure of the β Tubulin Dimer by Electron Crystallography. *Nature* **1998**, *391*, 199–203.
- (13) Lowe, J.; Li, H.; Downing, K. H.; Nogales, E. Refined Structure of α-β-Tubulin at 3.5 Å Resolution. *J. Mol. Biol.* **2001**, *313*, 1045–1057.
- (14) Combeau, C.; Commerçon, A.; Mioskowski, C.; Rousseau, B.; Aubert, F.; Goeldner, M. Predominant Labeling of β- over α-Tubulin from Porcine Brain by a Photoactivatable Taxoid Derivative. *Biochemistry* **1994**, *33*, 6676–6683.
- (15) Dasgupta, D.; Park, H.; Harriman, G. C.; Georg, G. I.; Himes, R. H. Synthesis of a Photoaffinity Taxol Analogue and Its Use in Labeling Tubulin. *J. Med. Chem.* **1994**, *37*, 2976–2980.

- (16) Rao, S.; Krauss, N. E.; Heerding, J. M.; Swindell, C. S.; Ringel, I.; Orr, G. A.; Horwitz, S. B. 3'-(*p*-Azidobenzamido)Taxol Photolabels the N-Terminal 31 Amino Acids of  $\beta$ -Tubulin. *J. Biol. Chem.* **1994**, *269*, 3132–3134.
- (17) Swindell, C. S.; Heerding, J. M.; Krauss, N. E.; Horwitz, S. B.; Rao, S.; Ringel, I. Characterization of Two Taxol Photoaffinity Analogues Bearing Azide and Benzophenone-Related Photoreactive Substituents in the A-Ring Side Chain. *J. Med. Chem.* **1994**, *37*, 1446–1449.
- (18) Rao, S.; Orr, G. A.; Chaudhary, A. G.; Kingston, D. G.; Horwitz, S. B. Characterization of the Taxol Binding Site on the Microtubule. 2-(*m*-Azidobenzoyl)taxol Photolabels a Peptide (Amino Acids 217–231) of  $\beta$ -Tubulin. *J. Biol. Chem.* **1995**, *270*, 20235–20238.
- (19) Loeb, C.; Combeau, C.; Ehret-Sabatier, L.; Breton-Gilet, A.; Faucher, D.; Rousseau, B.; Commerçon, A.; Goeldner, M. [3h]-(Azidophenyl)Ureido Taxoid Photolabels Peptide Amino Acids 281–304 of  $\alpha$ -Tubulin. *Biochemistry* **1997**, *36*, 3820–3825.
- (20) Díaz, J. F.; Valpuesta, J. M.; Chacon, P.; Diakun, G.; Andreu, J. M. Changes in Microtubule Protofilament Number Induced by Taxol Binding to an Easily Accessible Site. Internal Microtubule Dynamics. *J. Biol. Chem.* **1998**, *273*, 33803–33810.
- (21) Díaz, J. F.; Strobe, R.; Engelborghs, Y.; Souto, A. A.; Andreu, J. M. Molecular Recognition of Taxol by Microtubules. Kinetics and Thermodynamics of Binding of Fluorescent Taxol Derivatives to an Exposed Site. *J. Biol. Chem.* **2000**, *275*, 26265–26276.
- (22) Díaz, J. F.; Barasoain, I.; Souto, A. A.; Amat-Guerri, F.; Andreu, J. M. Macromolecular Accessibility of Fluorescent Taxoids Bound at a Paclitaxel Binding Site in the Microtubule Surface. *J. Biol. Chem.* **2005**, *280*, 3928–3937.
- (23) Buey, R. M.; Calvo, E.; Barasoain, I.; Pineda, O.; Edler, M. C.; Matesanz, R.; Cerezo, G.; Vanderwal, C. D.; Day, B. W.; Sorensen, E. J.; Lopez, J. A.; Andreu, J. M.; Hamel, E.; Díaz, J. F. Cyclostreptin Binds Covalently to Microtubule Pores and Lumenal Taxoid Binding Sites. *Nat. Chem. Biol.* **2007**, *3*, 117–125.
- (24) Magnani, M.; Maccari, G.; Andreu, J. M.; Díaz, J. F.; Botta, M. Possible Binding Site for Paclitaxel at Microtubule Pores. *FEBS J.* **2009**, *276*, 2701–2712.
- (25) Barasoain, I.; García-Carril, A. M.; Matesanz, R.; Maccari, G.; Trigili, C.; Mori, M.; Shi, J.-Z.; Fang, W.-S.; Andreu, J. M.; Botta, M.; Díaz, J. F. Probing the Pore Drug Binding Site of Microtubules with Fluorescent Taxanes: Evidence of Two Binding Poses. *Chem. Biol.* **2010**, *17*, 243–253.
- (26) Canales, A.; Rodríguez-Salarichs, J.; Trigili, C.; Nieto, L.; Coderch, C.; Andreu, J. M.; Paterson, I.; Jiménez-Barbero, J.; Díaz, J. F. Insights into the Interaction of Discodermolide and Docetaxel with Tubulin. Mapping the Binding Sites of Microtubule-Stabilizing Agents by Using an Integrated Nmr and Computational Approach. *ACS Chem. Biol.* **2011**, *6*, 789–799.
- (27) Chacón, P.; Wriggers, W. Multiresolution Contour-Based Fitting of Macromolecular Structures. *J. Mol. Biol.* **2002**, *317*, 375–384.
- (28) Case, D. A.; Cheatham, T. E., III; Darden, T.; Gohlke, H.; Luo, R.; Merz, K. M. J.; Onufriev, A.; Simmerling, C.; Wang, B.; Woods, R. J. The Amber Biomolecular Simulation Programs. *J. Comput. Chem.* **2005**, *26*, 1668–1688.
- (29) Pearlman, D. A.; Case, D. A.; Caldwell, J. W.; Ross, W. S.; Cheatham, T. E., III; DeBolt, S.; Ferguson, D.; Seibel, G.; Kollman, P. AMBER, a Package of Computer Programs for Applying Molecular Mechanics, Normal Mode Analysis, Molecular Dynamics and Free Energy Calculations to Simulate the Structural and Energetic Properties of Molecules. *Comput. Phys. Commun.* **1995**, *91*, 1–41.
- (30) Case, D. A.; Darden, T. A.; Cheatham III, T. E.; Simmerling, C. L.; Wang, J.; Duke, R. E.; Luo, R.; Walker, R. C.; Zhang, W.; Merz, K. M.; Roberts, B.; Wang, B.; Hayik, S.; Roitberg, A.; Seabra, G.; Kolossaváry, I.; Wong, K. F.; Paesani, F.; Vanicek, J.; Liu, J.; Wu, X.; Brozell, S. R.; Steinbrecher, T.; Gohlke, H.; Cai, Q.; Ye, X.; Wang, J.; Hsieh, M. J.; Cui, G.; Roe, D. R.; Mathews, D. H.; Seetin, M. G.; Saguia, C.; Babin, V.; Luchko, T.; Gusalov, S.; Kovalenko, A.; Kollman, P. A. AMBER 11; University of California: San Francisco, 2011.
- (31) Cheatham, T. E.; Srinivasan, J.; Case, D. A.; Kollman, P. A. Molecular Dynamics and Continuum Solvent Studies of the Stability of PolyG–PolyC and PolyA–PolyT DNA Duplexes in Solution. *J. Biomol. Struct. Dyn.* **1998**, *16*, 265–280.
- (32) Srinivasan, J.; Miller, J.; Kollman, P. A.; Case, D. A. Continuum Solvent Studies of the Stability of RNA Hairpin Loops and Helices. *J. Biomol. Struct. Dyn.* **1998**, *16*, 671–682.
- (33) Kollman, P. A.; Massova, I.; Reyes, C.; Kuhn, B.; Huo, S.; Chong, L.; Lee, M.; Lee, T.; Duan, Y.; Wang, W.; Donini, O.; Cieplak, P.; Srinivasan, J.; Case, D. A.; Cheatham, T. E. Calculating Structures and Free Energies of Complex Molecules: Combining Molecular Mechanics and Continuum Models. *Acc. Chem. Res.* **2000**, *33*, 889–897.
- (34) Schlitter, J.; Engels, M.; Krüger, P. Targeted Molecular Dynamics: A New Approach for Searching Pathways of Conformational Transitions. *J. Mol. Graph.* **1994**, *12*, 84–89.
- (35) Böhm, G. New Approaches in Molecular Structure Prediction. *Biophys. Chem.* **1996**, *59*, 1–32.
- (36) Díaz, J. F.; Wroblowski, B.; Schlitter, J.; Engelborghs, Y. Calculation of Pathways for the Conformational Transition between the GTP- and GDP-Bound States of the Ha-Ras-P21 Protein: Calculations with Explicit Solvent Simulations and Comparison with Calculations in Vacuum. *Proteins* **1997**, *28*, 434–51.
- (37) Snyder, J. P. The Microtubule-Pore Gatekeeper. *Nat. Chem. Biol.* **2007**, *3*, 81–82.
- (38) Freedman, H.; Huzil, J. T.; Luchko, T.; Ludueña, R. F.; Tuszyński, J. A. Identification and Characterization of an Intermediate Taxol Binding Site within Microtubule Nanopores and a Mechanism for Tubulin Isotype Binding Selectivity. *J. Chem. Inf. Model.* **2009**, *49*, 424–436.
- (39) Torrie, G. M.; Valleau, J. P. Nonphysical Sampling Distributions in Monte Carlo Free-Energy Estimation: Umbrella Sampling. *J. Comput. Phys.* **1977**, *23*, 187–199.
- (40) Beveridge, D. L.; DiCapua, F. M. Free Energy Via Molecular Simulation: Applications to Chemical and Biomolecular Systems. *Annu. Rev. Biophys. Biophys. Chem.* **1989**, *18*, 431–492.
- (41) Laio, A.; Parrinello, M. Escaping Free-Energy Minima. *Proc. Natl. Acad. Sci. U.S.A.* **2002**, *99*, 12562–12566.
- (42) Branduardi, D.; Gervasio, F. L.; Parrinello, M. From A to B in Free Energy Space. *J. Chem. Phys.* **2007**, *126*, 054103.
- (43) Bonomi, M.; Branduardi, D.; Gervasio, F. L.; Parrinello, M. The Unfolded Ensemble and Folding Mechanism of the C-Terminal Gb1  $\beta$ -Hairpin. *J. Am. Chem. Soc.* **2008**, *130*, 13938–13944.
- (44) Bonomi, M.; Branduardi, D.; Bussi, G.; Camilloni, C.; Provati, D.; Raiteri, P.; Donadio, D.; Marinelli, F.; Pietrucci, F.; Broglia, R. A.; Parrinello, M. Plumed: A Portable Plugin for Free-Energy Calculations with Molecular Dynamics. *Comput. Phys. Commun.* **2009**, *180*, 1961–1972.
- (45) Han, Y.; Chaudhary, A. G.; Chordia, M. D.; Sackett, D. L.; Perez-Ramirez, B.; Kingston, D. G.; Bane, S. Interaction of a Fluorescent Derivative of Paclitaxel (Taxol) with Microtubules and Tubulin-Colchicine. *Biochemistry* **1996**, *35*, 14173–14183.
- (46) Li, Y.; Edsall, R. J.; Jagtap, P. G.; Kingston, D. G.; Bane, S. Equilibrium Studies of a Fluorescent Paclitaxel Derivative Binding to Microtubules. *Biochemistry* **2000**, *39*, 616–623.
- (47) Czaplinski, K. H.; Grunewald, G. L. A Comparative Molecular Field Analysis Derived Model of the Binding of Taxol Analogue to Microtubules. *Bioorg. Med. Chem. Lett.* **1994**, *4*, 2211–2216.
- (48) Ojima, I.; Slater, J. C.; Michaud, E.; Kuduk, S. D.; Bounaud, P. Y.; Vrignaud, P.; Bissery, M. C.; Veith, J. M.; Pera, P.; Bernacki, R. J. Syntheses and Structure–Activity Relationships of the Second-Generation Antitumor Taxoids: Exceptional Activity against Drug-Resistant Cancer Cells. *J. Med. Chem.* **1996**, *39*, 3889–3896.
- (49) Zhu, Q.; Guo, Z.; Huang, N.; Wang, M.; Chu, F. Comparative Molecular Field Analysis of a Series of Paclitaxel Analogue. *J. Med. Chem.* **1997**, *40*, 4319–4328.
- (50) Duan, Y.; Wu, C.; Chowdhury, S.; Lee, M. C.; Xiong, G.; Zhang, W.; Yang, R.; Cieplak, P.; Luo, R.; Lee, T.; Caldwell, J.; Wang, J.; Kollman, P. A. Point-Charge Force Field for Molecular Mechanics

- Simulations of Proteins Based on Condensed-Phase Quantum Mechanical Calculations. *J. Comput. Chem.* **2003**, *24*, 1999–2012.
- (51) Jorgensen, W. L.; Chandrasekhar, J.; Madura, J. D.; Impey, R. W.; Klein, M. L. Comparison of Simple Potential Functions for Simulating Liquid Water. *J. Chem. Phys.* **1983**, *79*, 926–935.
- (52) Ryckaert, J. P.; Cicotti, G.; Berendsen, H. Numerical Integration of the Cartesian Equations of Motion of a System with Constraints: Molecular Dynamics of N-Alkanes. *J. Comput. Phys.* **1977**, *23*, 327.
- (53) Miyamoto, S.; Kollman, P. A. Settle—An Analytical Version of the Shake and Rattle Algorithm for Rigid Water Models. *J. Comput. Chem.* **1992**, *13*, 952–962.
- (54) Onufriev, A.; Bashford, D.; Case, D. A. Modification of the Generalized Born Model Suitable for Macromolecules. *J. Phys. Chem. B* **2000**, *104*, 3712–3720.
- (55) Onufriev, A.; Bashford, D.; Case, D. A. Exploring Protein Native States and Large-Scale Conformational Changes with a Modified Generalized Born Model. *Proteins* **2004**, *55*, 383–94.
- (56) Díaz, J. F.; Buey, R. M. Characterizing Ligand–Microtubule Binding by Competition Methods. *Methods Mol. Med.* **2007**, *137*, 245–260.
- (57) Hoops, S.; Sahle, S.; Gauges, R.; Lee, C.; Pahle, J. Á.; Simus, N.; Singhal, M.; Xu, L.; Mendes, P.; Kummer, U. Copasi—A Complex Pathway Simulator. *Bioinformatics* **2006**, *22*, 3067–3074.
- (58) Petzold, L. Automatic Selection of Methods for Solving Stiff and Nonstiff Systems of Ordinary Differential Equations. *SIAM J. Sci. Stat. Comput.* **1983**, *4*, 136–148.
- (59) Hindmarsh, A. C. Odepak, a Systematized Collection of Ode Solvers. *IMACS Trans. Sci. Comput.* **1983**, *1*, 55–64.